Quantitative Analysis of the Fate of Gold Nanocages In Vitro and In Vivo after Uptake by U87-MG Tumor Cells**

Eun Chul Cho, Yu Zhang, Xin Cai, Christine M. Moran, Lihong V. Wang, and Younan Xia**

Nanoparticles have been extensively used as carriers to deliver theranostic agents into tumors through the enhanced permeation and retention (EPR) effect,[1] and to regulate the release of a chemical or biological effector in response to environmental stimuli, such as temperature or pH change.[2] In these cases, cell uptake of nanoparticles has been studied to maximize their delivery into the target cells. Cell uptake of nanoparticles has also been extensively investigated in an effort to understand their cytotoxicity and potential societal impacts.[3] Many reports have demonstrated that the uptake of nanoparticles by cells depends on their sizes,[4] shapes,[5] and surface properties,[6] among others.[7] However, little attention has been given to monitoring the fate of nanoparticles in cells or tissues as a function of time, which should be of great importance in understanding the delivery efficiency and toxicity of nanoparticles. In a recent in vitro study, using a statistical method it was demonstrated that nanoparticles were distributed unequally in cells when these divided.[8] However, the conclusion was drawn from an analysis of a large number of cells rather than by tracking the nanoparticles in individual cells during their division. In addition, no such study has been reported for cells under in vivo conditions.

Herein we demonstrate two methods to monitor and quantitatively analyze the fate of Au nanocages (AuNCs) in U87-MG glioblastoma (brain tumor) cells under both in vitro and in vivo conditions. Figure 1 a shows a schematic depiction

of the objective of this study, that is, to quantitatively measure the distributions of AuNCs in cells as well as their clearance from the cells during proliferation. As a new class of nanoparticles with hollow interiors and porous walls, AuNCs have been extensively explored for biomedical applications, including imaging, diagnostics, controlled release, and therapeutics,[9] because of their surface plasmon resonance (SPR) properties.[10] Herein we used the two-photon luminescence properties[11a] and strong optical absorption[11b] of AuNCs to track and quantify them in the target cells or in a tumor.

We used AuNCs with an outer-edge length of approximately 50 nm for our study (Figure 1 b). They were prepared according to our previously published protocol.[12] Their surfaces were then functionalized with cyclic Arg-Gly-Asp-D-Tyr-Lys, c(RGDyK), a peptide that is capable of specifically targeting the integrin receptors on U87-MG cells (Figure 1 c).[13]

We first quantified the cellular uptake of c(RGDyK)-covered AuNCs by incubating them at various particle concentrations with U87-MG cells at 37°C for 24 hours. The average number of AuNCs taken up by an individual cell was then determined using a UV/Vis spectroscopic method (see Figure S1 in the Supporting Information).[14] The number of AuNCs that were taken up per cell increased linearly with an increasing particle concentration (Figure 1 d).

We then used two-photon microscopy (TPM) to examine the fate of the AuNCs that were taken up by the cells in vitro by calculating the number of AuNCs in each cell from the photoluminescence intensity. In this case, an incubation time of 24 hours was used to ensure that each cell would contain approximately 4.0×10^3 AuNCs. The cells were harvested by trypsin treatment and reseeded in a culture plate at a density of around 20 cells per plate. The seeded cells, referred to as mother cells, were then imaged individually using TPM, and the photoluminescence intensity from each cell was recorded and integrated. Because the doubling time for the U87-MG cells is approximately 48 hours, we were able to observe the divided cells (i.e., daughter cells) after the sample had been incubated for two days.

Figure 2 a shows a typical TPM image of a U87-MG mother cell at the time of seeding, and Figure 2 b shows a pair of daughter cells derived from this mother cell two days after seeding. A total of 14 mother cells and their 28 corresponding daughter cells were monitored (Figure S2). It is clear that all mother cells divided into two daughter cells within a period of two days. Although in some cases, a pair of daughter cells (e.g., in Figure 2 b) showed different degrees of stretching and thus different cellular areas, we assumed that they have equal volumes because this is usually the case when mammalian

[*] Dr. E. C. Cho,[$][+] Y. Zhang,[#][+] X. Cai,[+] C. M. Moran,[#]
Prof. L. V. Wang, Prof. Y. Xia[#]
Department of Biomedical Engineering
Washington University
St. Louis, MO 63130 (USA)
E-mail: younan.xia@bme.gatech.edu

[$] Current address: Department of Chemical Engineering
Division of Chemical and Bioengineering, Hanyang University
Seoul, 133-791 (Korea)

[#] Current address: The Wallace H. Coulter Department of Biomedical
Engineering, Georgia Institute of Technology and Emory University
Atlanta, GA 30332 (USA)

[+] These authors contributed equally to this work.

Supporting information for this article (including procedures for the synthesis of AuNCs, surface modification, and cell culture, two-photon microscopy, and photoacoustic imaging) is available on the WWW under http://dx.doi.org/10.1002/anie.201208096.
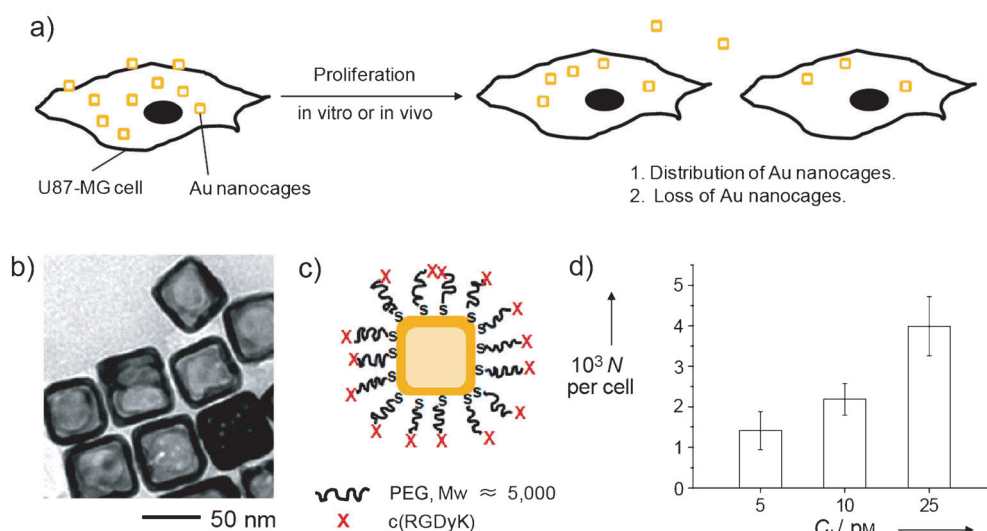
1152 WILEY ONLINE LIBRARY

© 2013 Wiley-VCH Verlag GmbH & Co. KGaA, Weinheim

Angew. Chem. Int. Ed. **2013**, *52*, 1152–1155

Figure 1. a) Quantitative analysis of the distributions of AuNCs in U87-MG brain tumor cells during their proliferation in vitro and in vivo. b) TEM image of AuNCs used for our experiments. c) Schematic representation of c(RGDyK)-labeled AuNCs. PEG = poly(ethylene glycol), X = cyclic RGD that can specifically bind to the integrin receptor on U87-MG cells. d) Number of AuNCs (N) taken up by U87-MG cells as a function of the concentration of AuNCs (C_I) incubated with the cells. The numbers were calculated from UV/Vis spectra of the supernatants with reference to a calibration curve.

cells divide. The photoluminescence intensity from each cell was used to determine the number of AuNCs in the cell through comparison with the calibration curve (Figure 2c). The average numbers of AuNCs per cell for the 14 mother cells and their corresponding 28 daughter cells after division is shown in Figure 2d. It is worth noting that the daughter cells did not equally share the AuNCs that were taken up by the mother cell (per volume) during the division of the mother cell ($p = 0.02$). When we added up the numbers of AuNCs in all daughter cells, the total was reduced by around $(20 \pm 8)\%$ relative to the number that was contained in their mother cells, suggesting that some of the AuNCs were cleared by the cells during the two-day culturing period. The decrease in Au content was further confirmed by analyzing the culture medium with inductively coupled mass spectrometry (ICP-MS). During the two-day culturing period, around 8% of the AuNCs re-entered into the culture medium. The drop in the number of AuNCs per cell could be attributed to the exocytosis and/or desorption of AuNCs that are bound to the surface of the cells.

We also monitored the c(RGDyK)-covered AuNCs in vivo using photoacoustic microscopy (PAM).[15] In this case, U87-MG cells containing approximately 4.0×10^3 AuNCs per cell were harvested by trypsin treatment and resuspended in a culture medium at a density of around 1×10^7 cells/mL. Next, 20 μL of the cell suspension were injected subcutaneously at the dorsal side of a nude mouse. Immediately after the injection, a PAM image of the cells in the nude mouse was acquired at an excitation wavelength of 770 nm, and the growth of

the tumor was monitored by PAM imaging every two days until six days after injection. Figure 3 shows time-lapse photographs of the tumor (indicated by the arrow) in the mouse (Figure 3a–d) and the corresponding PAM maximum amplitude projection (MAP) images (Figure 3e–h, X-Y plane; Figure 3i–l, X-Z plane; and Movies S1–S4, 3D reconstructions; the signals from blood vessels were removed). The photoacoustic amplitude for the tumor area gradually decreased over time. Meanwhile, the thickness of the tumor (i.e., depth in the direction from the surface of the skin into the tissue) greatly increased, leading to an increase in tumor volume from around 1.26 mm^3 to around 6.28 mm^3 in six days. By treating the explanted tumors (in parallel control groups)
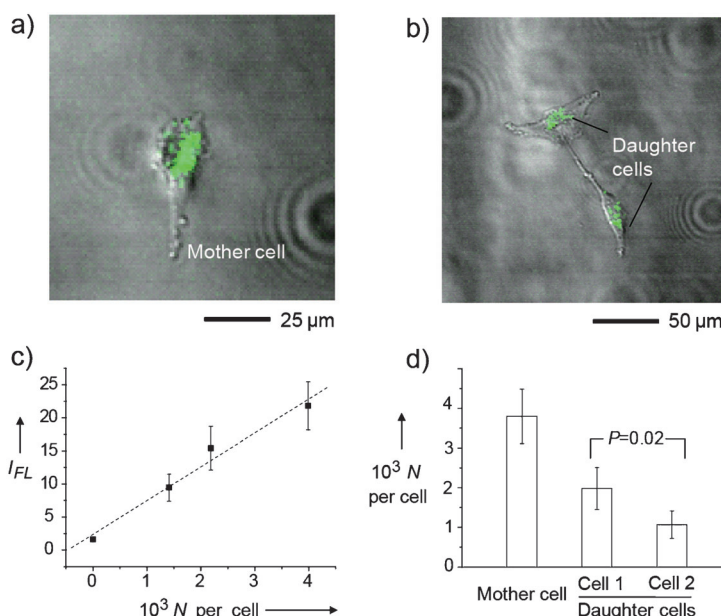

Figure 2. Superimposed two-photon and phase-contrast images showing a) a U87-MG mother cell and b) its two daughter cells after two days of culturing. The photoluminescence from AuNCs labeled with cyclic RGD is shown in green. c) Calibration curve for the photoluminescence intensity (I_{FL}) as a function of the number of AuNCs per cell (N) as obtained from the TPM images. The photoluminescence intensity and N showed a linear correlation. d) N in mother cells and their corresponding daughter cells after division. The data was obtained by averaging the intensities of 14 mother cells and their corresponding daughter cells (see Figure S2), respectively, and the intensities were converted to the number of AuNCs according to the calibration curve. The p value was obtained from analysis of variance (ANOVA).
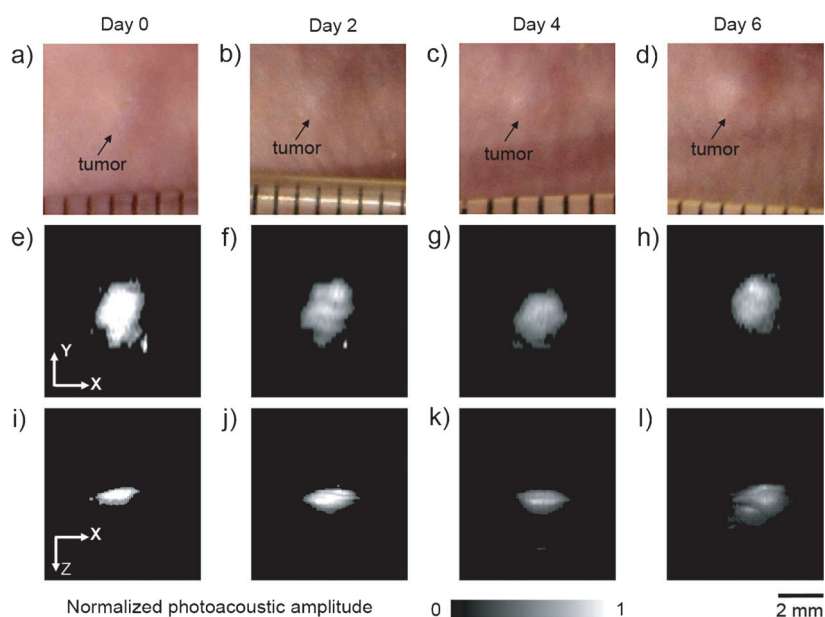
Figure 3. a–d) Time-lapse photographs showing a tumor growing on the dorsal side of a nude mouse after subcutaneous injection of U87-MG cells containing AuNCs. The tumor was non-invasively monitored up to six days after injection using PAM. e–l) Time-lapse in vivo PAM MAP images of the tumor growing in the same nude mouse. The cells initially contained approximately 4×10^3 AuNCs per cell. MAP = maximum amplitude projection.

In addition, the standard deviation of the number of AuNCs per cell in the entire cell population over time represented the distribution of the AuNCs in the cells or the tumor during their proliferation. Table 2 shows the percentage standard deviation relative to the number of AuNCs per cell obtained from UV/Vis, TPM, and PAM. On day 0, the percentages obtained from the three techniques were in good agreement with each other (with variations in the range of 18–20%). The percentages increased over time both in vitro and in vivo. The increasing value of standard deviation implies that the number of AuNCs in the cells or in the tumor differed increasingly among the cells during their proliferation. In other words, this result suggests that the cells likely did not share the AuNCs equally when they divided.

In conclusion, we have quantitatively analyzed the fate of target-specific AuNCs in a brain tumor cell line both in vitro and in vivo. As a novel class of nanoparticles with hollow interiors and porous walls, AuNCs are finding wide use in drug delivery and cancer therapeutics.[9] The tunable scattering and absorption peaks of AuNCs in the near-

with a combination of collagenase and trypsin, the number of tumor cells increased from around 2.0×10^5 to around 9.4×10^5 in six days.

Based on the PAM images shown in Figure 3, we estimated the total number of AuNCs (N_{total}) within the tumor at each time point. We first obtained a calibration curve for in vivo conditions (Figure 4a and Figure S3). The photoacoustic amplitude, which was averaged from the entire region of the proliferating tumor at each time point (Figure 4b), was then converted to the number of AuNCs per cell based on the calibration curve. By multiplying the number of nanocages per cell by the number of tumor cells at each time point, we were able to estimate N_{total} in the tumor. N_{total} decreased by approximately $(12 \pm 10)\%$ in six days (Figure 4c), implying that the AuNCs were likely cleared from the cells and then carried away from the tumor site through blood flow. However, the decrease in N_{total} did not linearly correlate with time. Instead, N_{total} decreased rapidly in the first two days and then stabilized until day six.

The present study provides an important, quantitative understanding of the distribution and clearance of AuNCs in U87-MG tumor cells both in vitro and in vivo. A plot of N_{total} as a function of time indicates that some of the AuNCs that were taken up by the cells were cleared by the cells over time (Table 1). We determined the percentage of reduction in N_{total} by ICP-MS, TPM, and PAM. In general, the cells or tumor lost approximately 10–20% of the initial AuNCs over a period of two to six days both in vitro and in vivo. This data suggests that the clearance of AuNCs from the tumor cells did not vary significantly, whether the cells were grown in vitro or in vivo for the period of time tested (4–6 days).

Table 1: Percentages of AuNCs cleared from the cells.[a]

	AuNCs cleared from cells [%]		
	Day 2	Day 4	Day 6
ICP-MS (in vitro)[b]	8	—[e]	—[e]
TPM (in vitro)[c]	20±8	—[e]	—[e]
PAM (in vivo)[d]	12±10	8±6	16±4

[a] At day 0, immediately after cell uptake, all the mother cells contained roughly the same number of AuNCs, about 4×10^3 per cell. [b] The number of mother cells used for the measurement was around 3×10^5. [c] The number of mother cells used for the measurement was 20. [d] The number of cells used for the measurement was around 2×10^5. [e] Not measured, because the in vitro studies were only conducted over a period of two days, during which the number of cells was doubled.

Table 2: Percentages of standard deviation (STD) for the average number of AuNCs per cell in the entire cell population.[a]

	Standard deviation [%]			
	Day 0	Day 2	Day 4	Day 6
UV/Vis (in vitro)[b]	18.3	—[e]	—[e]	—[e]
TPM (in vitro)[c]	18	42	—[f]	—[f]
PAM (in vivo)[d]	20	29	31	38

[a] At day 0, immediately after cell uptake, all mother cells contained roughly the same number of AuNCs, about 4×10^3 per cell. [b] The number of mother cells used for the measurement was around 3×10^5. [c] The number of mother cells used for the measurement was 20. [d] The number of cells used for the measurement was around 2×10^5. [e] Not detected, because of limitations of the technique. [f] Not measured, because in vitro studies were only conducted over a period of two days, during which the number of cells was doubled.
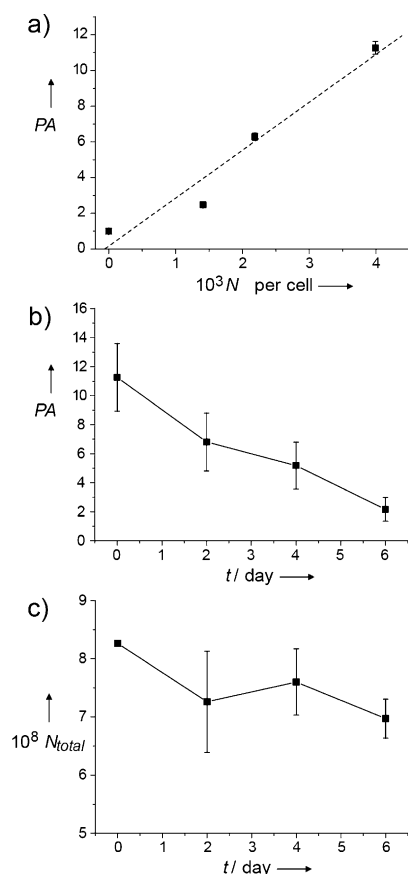
Figure 4. a) Calibration curve for photoacoustic amplitude (*PA*) as a function of the number of AuNCs in U87-MG cells. Four sets of cells containing different numbers of nanocages per cell were injected subcutaneously into the dorsal side of a nude mouse, and the photoacoustic amplitudes were obtained in vivo immediately after injection of the cells. The amplitudes were linearly proportional to the number of nanocages in the cells. b) Change in the photoacoustic amplitude of the tumor containing AuNCs and growing in a nude mouse over time. c) Total number of AuNCs (N_{total}) estimated from PAM data as a function of tumor growth time by multiplication of the number of AuNCs per cell (calculated from the calibration curve) and the number of cells at each time point.

infrared region also make them excellent contrast agents for a number of optical imaging methods. All of these applications require a quantitative understanding of the fate of nanoparticles once they have been delivered into cells. In the present study, by using TPM and PAM, it was found that cells did not share the AuNCs equally during their division. We believe that a comparison between the fate of AuNCs in in vitro and in vivo studies could also provide useful information on the biological activities of tumor cells under different physiological conditions. The present study is important for future studies involving nanoparticles for biomedicine and nanotoxicology, in which it is critical to know the delivery efficiency and/or the fate of nanoparticles in cells during prolonged periods of proliferation.

[1] a) P. Ghosh, G. Han, M. De, C. K. Kim, V. M. Rotello, *Adv. Drug Delivery Rev.* **2008**, *60*, 1307–1315; b) H. Maeda, J. Wu, T. Sawa, Y. Matsumura, K. Hori, *J. Controlled Release* **2000**, *65*, 271–284.

[2] a) R. M. Sawant, J. P. Hurley, S. Salmaso, A. Kale, E. Tolcheva, T. S. Levchenko, V. P. Torchilin, *Bioconjugate Chem.* **2006**, *17*, 943–949; b) A. Rösler, G. W. M. Vandermeulen, H.-A. Klok, *Adv. Drug Delivery Rev.* **2001**, *53*, 95–108.

[3] a) A. Nel, T. Xia, L. Madler, N. Li, *Science* **2006**, *311*, 622–627; b) J. G. Teeguarden, P. M. Hinderliter, G. Orr, B. D. Thrall, J. G. Pounds, *Toxicol. Sci.* **2007**, *95*, 300–312; c) D. Lison, L. C. J. Thomassen, V. Rabolli, L. Gonzalez, D. Napierska, J. W. Seo, M. Kirsch-Volders, P. Hoet, C. E. A. Kirschhock, *Toxicol. Sci.* **2008**, *104*, 155–162.

[4] a) W. Jiang, B. Y. S. Kim, J. T. Rutka, W. C. W. Chan, *Nat. Nanotechnol.* **2008**, *3*, 145–150; b) A. P. Alivisatos, W. Gu, C. Larabell, *Annu. Rev. Biomed. Eng.* **2005**, *7*, 55–76; c) J. Rejman, V. Oberle, I. S. Zuhorn, D. Hoekstra, *Biochem. J.* **2004**, *377*, 159–169; d) J. Panyam, V. Labhasetwar, *Adv. Drug Delivery Rev.* **2003**, *55*, 329–347; e) S. Prabha, W.-Z. Zhou, J. Panyam, V. Labhasetwar, *Int. J. Pharm.* **2002**, *244*, 105–115.

[5] a) E. C. Cho, L. Au, Q. Zhang, Y. Xia, *Small* **2010**, *6*, 517–522; b) B. D. Chithrani, W. C. W. Chan, *Nano Lett.* **2007**, *7*, 1542–1550.

[6] a) A. Verma, F. Stellacci, *Small* **2010**, *6*, 12–21; b) A. Verma, O. Uzun, Y. Hu, Y. Hu, H.-S. Han, N. Watson, S. Chen, D. J. Irvine, F. Stellacci, *Nat. Mater.* **2008**, *7*, 588–595; c) P. R. Leroueil, S. Hong, A. Mecke, J. R. Baker, Jr., B. G. Orr, M. M. B. Holl, *Acc. Chem. Res.* **2007**, *40*, 335–342; d) E. C. Cho, J. Xie, P. A. Wurm, Y. Xia, *Nano Lett.* **2009**, *9*, 1080–1084; e) M. Zorko, U. Langel, *Adv. Drug Delivery Rev.* **2005**, *57*, 529–545; f) J. Sudimack, R. J. Lee, *Adv. Drug Delivery Rev.* **2000**, *41*, 147–162.

[7] a) A. Alexandre, W. C. W. Chan, *ACS Nano* **2011**, *5*, 5478–5489; b) J. Lin, H. Zhang, Z. Chen, Y. Zheng, *ACS Nano* **2010**, *4*, 5421–5429; c) K. V. Chakravarthy, A. C. Bonoiu, W. G. Davis, P. Ranjan, H. Ding, R. Hu, J. B. Bowzard, E. J. Bergey, J. M. Katz, P. R. Knight, S. Sambhara, P. N. Prasad, *Proc. Natl. Acad. Sci. USA* **2010**, *107*, 10172–10177; d) E. Hutter, S. Boridy, S. Labrecque, M. Lalancette-Hebert, J. Kriz, F. M. Winnik, D. Maysinger, *ACS Nano* **2010**, *4*, 2595–2606.

[8] H. D. Summers, P. Rees, M. D. Holton, M. R. Brown, S. C. Chappell, P. J. Smith, R. J. Errington, *Nat. Nanotechnol.* **2011**, *6*, 170–174.

[9] Y. Xia, W. Li, C. M. Cobley, J. Chen, X. Xia, Q. Zhang, M. Yang, E. C. Cho, P. K. Brown, *Acc. Chem. Res.* **2011**, *44*, 914–924.

[10] J. Chen, B. Wiley, Z.-Y. Li, D. Campbell, F. Saeki, H. Cang, L. Au, J. Lee, X. Li, Y. Xia, *Adv. Mater.* **2005**, *17*, 2255–2261.

[11] a) L. Au, Q. Zhang, C. M. Cobley, M. Gidding, A. G. Schwartz, J. Chen, Y. Xia, *ACS Nano* **2010**, *4*, 35–42; b) E. C. Cho, C. Kim, F. Zou, C. M. Cobley, K. H. Song, J. Chen, Z.-Y. Li, L. V. Wang, Y. Xia, *J. Phys. Chem. C* **2009**, *113*, 9023–9028.

[12] S. E. Skrabalak, L. Au, X. Li, Y. Xia, *Nat. Protoc.* **2007**, *2*, 2182–2190.

[13] X. Chen, R. Park, M. Tohme, A. H. Shahinian, J. R. Bading, P. S. Conti, *Bioconjugate Chem.* **2004**, *15*, 41–49.

[14] a) E. C. Cho, Y. Liu, Y. Xia, *Angew. Chem.* **2010**, *122*, 2020–2024; *Angew. Chem. Int. Ed.* **2010**, *49*, 1976–1980; b) E. C. Cho, Q. Zhang, Y. Xia, *Nat. Nanotechnol.* **2011**, *6*, 385–391.

[15] a) H. F. Zhang, K. Maslov, G. Stoica, L. V. Wang, *Nat. Biotechnol.* **2006**, *24*, 848–851; b) C. Kim, E. C. Cho, J. Chen, K. H. Song, L. Au, C. Favazza, Q. Zhang, C. M. Cobley, F. Gao, Y. Xia, L. V. Wang, *ACS Nano* **2010**, *4*, 4559–4564.